8-fs pulses from a compact Er:fiber system: quantitative modeling and experimental implementation

Alexander Sell, Günther Krauss, Rüdiger Scheu, Rupert Huber, and Alfred Leitenstorfer

Department of Physics and Center for Applied Photonics
University of Konstanz, 78457 Konstanz, Germany
alfred.leitenstorfer@uni-konstanz.de

Abstract: We demonstrate an all-fiber turnkey source of extremely stable 2-cycle pulses at a center wavelength of 1.17 μm. Taylor-cut highly nonlinear germano-silica bulk fibers (HNFs) provide smooth supercontinua with a bandwidth of 560 nm and a spectral shape precisely controlled by the dispersion of the fiber and the phase of the 1.55 μm pump pulses. Alternatively these fibers are capable of generating pulses with central wavelengths continuously tunable from 0.9 μm up to 1.4 μm. These results are based on parameter-free simulations of nonlinear pulse propagation including higher-order dispersion as well as instantaneous Kerr and retarded Raman contributions.

OCIS codes: (320.7090) Ultrafast lasers; (060.4370) Nonlinear optics, fibers; (320.6629) Supercontinuum generation; (320.7140) Ultrafast processes in fibers.

References and links

1. G. Steinmeyer, D. H. Sutter, L. Gallmann, N. Matuschek, and U. Keller, "Frontiers in Ultrashort Pulse Generation: Pushing the Limits in Linear and Nonlinear Optics," Science **286**, 1507-1512 (1999).
2. C. Kübler, R. Huber, S. Tübel and A. Leitenstorfer, "Ultrabroadband detection of multi-THz field transients with GaSe electro-optic sensors: approaching the near infrared," Appl. Phys. Lett. **85**, 3360-3362 (2004).
3. T. Brabec and F. Krausz, "Intense few-cycle laser fields: Frontiers of nonlinear optics," Rev. Mod. Phys. **72**, 545-591 (2000).
4. S. Rausch, T. Binhammer, A. Harth, J. Kim, R. Ell, F. X. Kärtner, and U. Morgner, "Controlled waveforms on the single-cycle scale from a femtosecond oscillator," Opt. Express **16**, 9739-9745 (2008).
5. L. Xu, G. Tempea, A. Poppe, M. Lenzner, C. Spielmann, F. Krausz, A. Stingl, and K. Ferencz, "High-power sub-10-fs ti:sapphire oscillators," Appl. Phys. B **65**, 151-159 (1997).
6. W. J. Wadsworth, A. Ortigosa-Blanch, J. C. Knight, T. A. Birks, T.-P. M. Man, and P. St. J. Russell, "Supercontinuum generation in photonic crystal fibers and optical fiber tapers: a novel light source," J. Opt. Soc. Am. B **19**, 2148-2155 (2002).
7. A. V. Husakou, and J. Herrmann, "Supercontinuum Generation of Higher-Order Solitons by Fission in Photonic Crystal Fibers," Phys. Rev. Lett. **87**, 203901 (2001).
8. K. Tamura, E. P. Ippen, H. A. Haus, and L. E. Nelson, "77-fs pulse generation from a stretched-pulse mode-locked all-fiber ring laser," Opt. Lett. **18**, 1080-1082 (1993).
9. J. Herrmann, U. Griebner, N. Zhavoronkov, A. Husakou, D. Nickel, J. C. Knight, W. J. Wadsworth, P. St. J. Russell, and G. Korn, "Experimental evidence for supercontinuum generation by fission of higher-order solitons in photonic fibers," Phys. Rev. Lett. **88**, 173901 (2002).
10. J. T. Gopinath, H. M. Shen, H. Sotobayashi, E. P. Ippen, T. Hasegawa, T. Nagashima, and N. Sugimoto, "Highly nonlinear bismuth-oxide fiber for smooth supercontinuum generation at 1.5 μm," Opt. Express **12**, 5697-5702 (2004).
11. J. Takayanagi, N. Nishizawa, T. Sugiura, M. Yoshida, and T. Goto, "Generation of Pedestal-Free 22-fs Ultrashort Pulse Using Highly Nonlinear Fiber and Reverse-Dispersion Fiber," IEEE J. Quantum Electron. **42**, 287-291 (2006).

#103469 - $15.00 USD Received 30 Oct 2008; revised 11 Dec 2008; accepted 11 Dec 2008; published 15 Jan 2009

12. T. Hori, N. Nishizawa, T. Goto, and M. Yoshida, "Experimental and numerical analysis of widely broadened supercontinuum generation in highly nonlinear dispersion-shifted fiber with a femtosecond pulse," J. Opt. Soc. Am. B **21**, 1969-1980 (2004).
13. F. Tauser, F. Adler, and A. Leitenstorfer, "Widely tunable sub-30-fs pulses from a compact erbium-doped fiber source," Opt. Lett. **29**, 516-518 (2004).
14. F. Adler, A. Sell, F. Sotier, R. Huber, and A. Leitenstorfer, "Attosecond relative timing jitter and 13 fs tunable pulses from a two-branch femtosecond Er:fiber laser," Opt. Lett. **32**, 3504-3506 (2007).
15. D. Träutlein, F. Adler, K. Moutzouris, A. Jeromin, A. Leitenstorfer, and E. Ferrando-May, "Highly versatile confocal microscopy system based on a tunable femtosecond Er : fiber source," J. Biophoton. **1**, 53-61 (2008).
16. P. V. Mamyshev und S. V. Chernikov, "Ultrashort-pulse propagation in optical fibers," Opt. Lett. **15**, 1076-1078 (1990).
17. R. H. Stolen, J. P. Gordon, W. J. Tomlinson, and H. A. Haus, "Raman response function of silica-core fibers," J. Opt. Soc. Am. B **6**, 1159-1166 (1989).
18. R. Trebino and D. J. Kane, "Using phase retrieval to measure the intensity and phase of ultrashort pulses: frequency-resolved optical gating," J. Opt. Soc. Am. A **10**, 1101-1111 (1993).
19. K. Moutzouris, F. Adler, F. Sotier, D. Träutlein, and A. Leitenstorfer, "Multimilliwatt ultrashort pulses continuously tunable in the visible from a compact fiber source," Opt. Lett. **31**, 1148-1150 (2006).

1. Introduction

Since the invention of the first mode locked laser there has been an ongoing demand for femtosecond pulses of ever shorter duration [1]. Increased bandwidth, tunability and temporal resolution have facilitated a wide range of applications such as pump-probe spectroscopy, field-resolved sampling of high frequency terahertz pulses [2], frequency metrology, optical coherence tomography and extreme nonlinear optics culminating in new avenues in attophysics [3].

Today sophisticated schemes of intra-cavity dispersion control facilitate the extraction of 2-cycle pulses directly from Ti:sapphire oscillators [4, 5]. Spectral broadening in microstructured fibers, tapers and gases with subsequent adaptive recompression is another means for generating broadband spectra in the Ti:sapphire spectral range [6, 7].

In the early 1990s the emergence of fiber lasers established a new technology with the potential to circumvent the noise issues and to extend the wavelength range into the infrared [8]. Yet Er:fiber oscillators are limited to the 100-fs-regime due to low gain bandwidths of fibers doped with rare earth ions. Several amplification and compression schemes have been proposed to broaden the spectra and to overcome the limitations [9–12], but the performance of Ti:sapphire lasers has still been out of reach.

In this letter we present a versatile laser source of widely tunable ultrashort output pulses entirely based on telecom-compatible fibers [13]. A noteworthy advantage of these waveguides is their superiour noise performance (see chapter 4 and Ref. 14). The key element of our system is a two-stage assembly of a precompression fiber spliced to a highly nonlinear bulk fiber for supercontinuum generation. The pulse formation within these optical elements includes dispersive propagation and self-phase modulation (SPM) as well as higher order effects such as optical shock front generation and the retarded $\chi^{(3)}$ response due to Raman-scattering. Quantitative simulations based on a modified nonlinear Schrödinger equation (NLSE) without free parameters allow us to design fibers for tailor-cut spectral and temporal pulse characteristics. By choosing the adequate dispersion profiles of the nonlinear optics, pulses with tunable central wavelengths between 1.4 μm and 0.9 μm are generated. We also demonstrate supercontinua featuring a spectral FWHM of 560 nm which are recompressed to a duration of 7.8 fs at an energy of 0.7 nJ. To our knowledge, these are the shortest pulses ever generated with fiber laser technology.

Fig. 1 depicts a schematic layout of the laser system. We start with a compact polarization mode-locked femtosecond Er:fiber master oscillator (OSC, repetition rate 49 MHz) [8] seeding a low-noise amplifier (EDFA) based on an erbium-doped gain fiber of a length of 1.75 m [13]. Pulses with energies up to 8 nJ are coupled into free space and recompressed to a duration

#103469 - $15.00 USD Received 30 Oct 2008; revised 11 Dec 2008; accepted 11 Dec 2008; published 15 Jan 2009

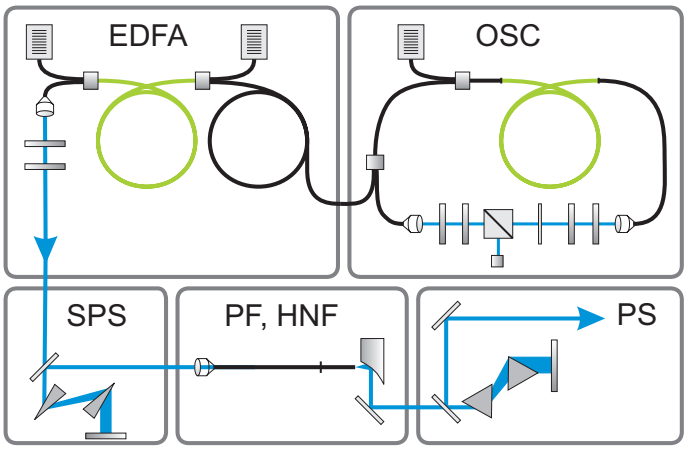

Fig. 1. Schematical setup of the laser system. OSC: Er:fiber oscillator, Kerr rotation mode-locked [8]; EDFA: Er:fiber amplifier consisting of pre-stretch fiber, single-mode gain fiber and waveplates for polarization control [13]; SPS: silicon prism sequence for pre-chirp control; PF: pre-compression fiber with collimating lens; HNF: bulk highly nonlinear silica fiber for supercontinuum generation; PS: SF10 prism sequence.

of 70 fs in a silicon prism sequence (SPS). A highly nonlinear bulk fiber (HNF) is directly spliced to a precompression fiber (PF). A standard fiber coupled telecom lens in a rigid housing in combination with the large mode area of the PF render the setup largely immune to beam-pointing instabilities induced by environmental noise (see below). The prechirp is used to tune the output wavelengths of the system as discussed in Ref. 13. Finally the pulses are coupled into free space again and recompressed in an SF10 prism sequence (PS).

2. Theoretical modeling and numerical simulations

Our first goal was to improve the laser for real-world applications such as time-resolved confocal microscopy [15] by extending the tuning range to wavelengths below 1 μm. To this end, a theoretical understanding of the processes within the nonlinear stage is required. Ultrashort pulse propagation in nonlinear fibers has been shown to be well described by a generalized NLSE [16]:

$$\partial_z A(z,\tau) = \left[-\frac{\alpha}{2} - i\frac{\beta_2}{2}\partial_\tau^2 + i\frac{\beta_3}{6}\partial_\tau^3 \pm \ldots\right] A(z,\tau) \qquad (1)$$
$$+\gamma\left(i - \frac{\partial_\tau}{\omega_0}\right)\left[A(z,\tau)\int_{-\infty}^{+\infty}|A(z,\tau_1)|^2 R(\tau-\tau_1)d\tau_1\right]$$

where $A(z,\tau)$ is the electric field envelope at the fiber position z and the retarded time τ in a frame moving with the group velocity of the pulse. The first parenthesis accounts for linear pulse propagation, parameterized by damping α and the dispersion coefficients β_n. Here, β_n denotes the n-th coefficient of the Taylor expansion of the propagation constant β around the center frequency ω_0. The second parenthesis includes the nonlinearities, quantified through $\gamma = (n_2\omega_0)/(cA_{\text{eff}})$ with the nonlinear refractive index n_2 and the effective mode field area A_{eff}. $R(\tau) = (1-f_{\text{R}})\,\delta(\tau) + f_{\text{R}}\,h_{\text{R}}(\tau)\,\Theta(\tau)$ includes the delta-like behaviour of the quasi-instantaneos Kerr response as well as the retarded Raman response at positive time τ [17].

#103469 - $15.00 USD Received 30 Oct 2008; revised 11 Dec 2008; accepted 11 Dec 2008; published 15 Jan 2009

It is instructive to define effective length scales on which different terms of Eq. 1 are operating: With the pulse width T_0, $L_{\mathrm{GVD}} \equiv T_0^2/|\beta_2|$ and $L_{\mathrm{TOD}} \equiv T_0^3/|\beta_3|$ are the length scales for linear dispersion and $L_{\mathrm{NL}} \equiv (P_0\,\gamma)^{-1}$ governs the nonlinear part. The degree of nonlinearity of the propagation is defined by introducing the ratio $N^2 \equiv L_{\mathrm{GVD}}/L_{\mathrm{NL}}$. For sech shaped pulses, integer values of N lead to Nth order solitons.

We employ a symmetric split-step Fourier scheme to numerically solve Eq. 1. For efficient calculation, nonlinearities are treated by a fourth order Runge-Kutta solver in the time domain employing discrete convolutions for fast integration. On a standard desktop computer a typical full simulation run completes within a second, allowing us to explore a broad parameter space while optimizing our nonlinear fiber setup.

In order to correctly describe the propagation of the extreme-bandwidth supercontinuum in the HNF we include linear dispersion up to 6$^{\mathrm{th}}$ order. A white-light interferometer gives experimental access to these parameters using fiber samples as short as 10 cm. Input pulse envelopes are retrieved in amplitude and phase via frequency resolved optical gating [18]. The nonlinearity γ is calculated from the fiber geometry, and the Raman contribution is taken from Ref. 17.

3. Generation of widely tunable spectra

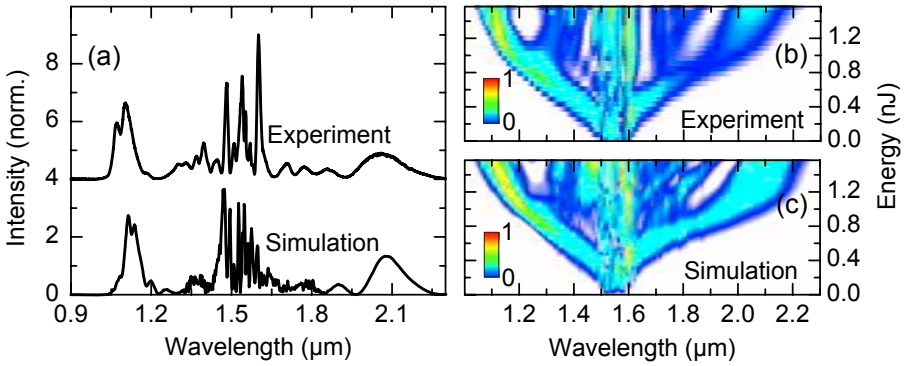

Fig. 2. (a) Output spectrum of tunable supercontinuum stage versus wavelength (top) and corresponding quantitative simulation employing retrieved pump spectrum and measured fiber dispersion (bottom); (b) experimental and (c) theoretical output spectra as functions of the pump pulse energy.

Fig. 2(a) displays a supercontinuum measured after a fiber compressor without additional optimization measures, pumped at a pulse energy of 1.42 nJ (upper part) and the corresponding simulation (lower part). No fit parameters were assumed in the numerical treatment, rendering the excellent agreement an indicator for the predictive power of our model. Both prominent peaks at the spectral edges are reproduced in their structure and relative amplitude. Also the spectral positions of the small oscillations between these maxima and the pump wavelength of 1.55 μm are replicated. An even more compelling test of the model is given in Fig. 2(b). By varying the pump pulse energy while at the same time recording the output spectra (color coded), the consistency of the calculations is tested over a broad range of input parameters. The HNF used in this experiment is strongly dispersion shifted and exhibits a measured zero dispersion wavelength (ZDW) of $\lambda_{\mathrm{ZD}} = 1.54$ μm well within the pump spectrum. It is fusion spliced to a precompression fiber ($\lambda_{\mathrm{ZD}} = 1.33$ μm). Our analysis shows, that this PF essentially supports solitonic compression (SC) at a soliton order of N = 1.9 and a

#103469 - $15.00 USD Received 30 Oct 2008; revised 11 Dec 2008; accepted 11 Dec 2008; published 15 Jan 2009

soliton period of $L_S \equiv L_{GVD}$ = 330 mm at a pump energy of 1.42 nJ. The compression factor $F_C \equiv t_{input}/t_{output}$ = 2.8 corresponds to an output pulse duration of t_{FWHM} = 30 fs while the temporal pulse shape is significantly cleaned up. When entering the HNF, this pulse immediately undergoes spectral broadening due to self phase modulation, generating two spectrally distinct peaks. The basic mechanism is similar to the soliton fission effect, first discussed for photonic crystal fibers [7, 9]: One of these peaks propagates in the anomalous dispersion regime, forming a long wave soliton, while the other one is emitted in the dispersive wavelength range and therefore suffers temporal broadening. Both pulses interact via four-wave-mixing which results in additional spectral repulsion. By analyzing the temporal evolution of these two pulses we find that the spectral broadening is limited by the group velocity mismatch between both pulses leading to a loss of temporal overlap after a propagation length of 30 mm of HNF. At this point the dispersive pulse is trailing the soliton and has a significantly reduced peak power due to dispersive stretching.

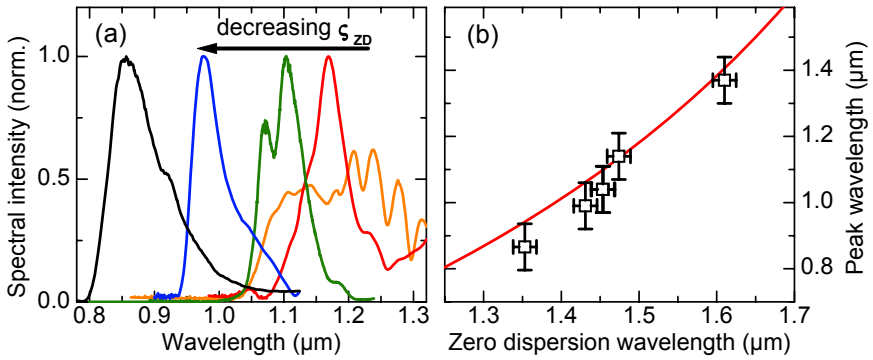

Fig. 3. (a) Experimentally determined intensity of the short-wave peak versus wavelength for various fibers with differing zero dispersion wavelength λ_{ZD}; (b) shortest experimental output peak wavelengths for various HNFs versus zero dispersion wavelength (squares) and theoretically predicted scaling of the dispersive wave central wavelength (solid line).

In order to increase the tuning range we design a dispersion profile allowing both pulses to perfectly overlap in time. By blue-shifting the point of maximum group velocity (i.e. reducing the ZDW), the long-wave part is slowed down allowing the short-wave part to catch up. This leads to an efficient interaction between both components within the first few millimeters of the HNF, leading to a much more rapid spectral separation. Since the pump spectrum is injected in a regime with anomalous dispersion, one may also speak of solitonic compression. First optimizations have resulted in the spectral extension shown in Fig. 3(a). Fig. 3(b) gives the experimental wavelength positions of the short-wave peaks as a function of the ZDW for various fibers (squares), clearly following the trend predicted by our numerical calculations (solid line). The broadest spectral range was covered using a nonlinear fiber with $\lambda_{ZD} = 1.35\ \mu$m. The output is tunable to a central wavelength as short as 856 nm [black curve in Fig. 3(a)]. We note that frequency doubling of this configuration results in ultrashort pulses tunable over the entire visible range [19].

4. Generation of 8-fs Pulses

With the reliability and predictive power demonstrated for our simulation tool, we will now go ahead and design a system generating the shortest pulse durations achieved with a fiber laser to date. We aim for few-cycle pulses with unstructured and stable spectra which are well suited as seed and gating pulses for state-of-the-art experiments. It turns out that a sufficiently short HNF

#103469 - $15.00 USD Received 30 Oct 2008; revised 11 Dec 2008; accepted 11 Dec 2008; published 15 Jan 2009

in our two-stage compressor provides the broadest spectral bandwidth of the dispersive peak. This observation corresponds to exploiting high-order SC with low dispersive distortions in the HNF. Fig. 4(a) depicts the pulse power (color coded) as a function of time and propagation length for a 9-cm-long PF pumped with slightly chirped Gaussian pulses (duration: 100 fs, energy: 5.0 nJ). Corresponding spectra for this stage are given in Fig. 4(b). Our simulations predict compression down to a FWHM pulse duration of 23 fs in the precompressor [Fig. 4(a) and black line in Fig. 4(c)]. Effective length scales for GVD (TOD) are represented as dashed (dotted) curves in Fig. 4(c). They decrease from 1200 mm (31 m) down to 28 mm (104 mm), indicating that TOD does not play an important role in this scheme. The nonlinearity N^2 is multiplied by 1 mm to be shown on the same scale (dash-dotted). It turns out that the soliton order exceeds $N = 6$.

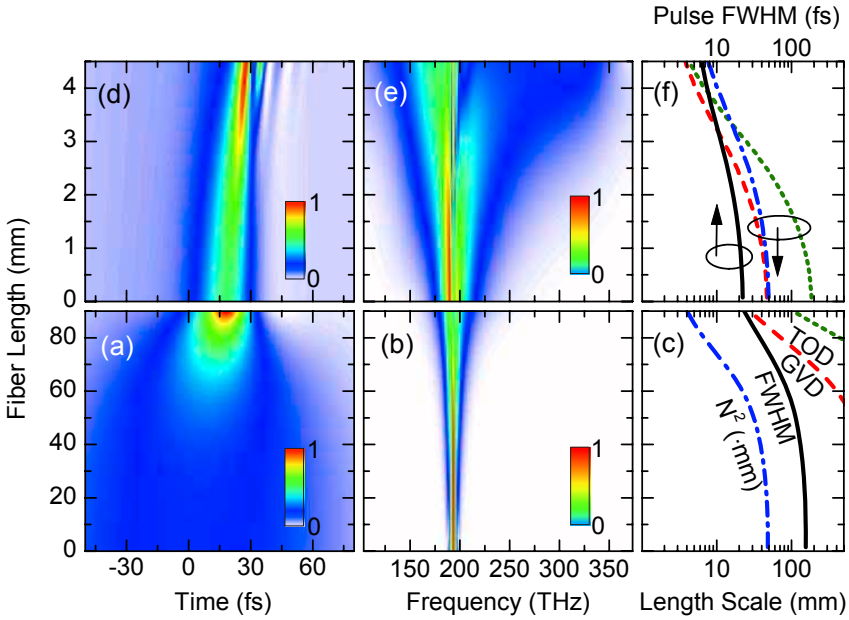

Fig. 4. Simulated pulse propagation within fiber compressor; (a)-(c) precompression of the pulse in a standard telecom fiber PF; (d)-(f) compression within a dispersion optimized highly nonlinear fiber HNF; (a, d) temporal power profile and (b, e) spectral intensity of the pulse vs. propagation length; (c, f) evolution of the FWHM pulse width (black line), the effective nonlinearity N^2 mm (blue, dash-dotted) and the GVD (red, dashed) and TOD (green, dotted) effective length scales (see text for details).

A similar analysis is given for the HNF of a length of 4.5 mm in Fig. 4(d)-(f). In the time domain [Fig. 4(d)] the pulse compresses further and develops oscillatory features at the trailing edge. Windowed Fourier transforms (not shown) indicate that the oscillations are due to influences of TOD on the short-wave peak whereas the solitonic part manifests itself near time zero. Our model predicts a duration of 6.4 fs of the anti-Stokes component without any additional compression. Fig. 4(e) shows the build-up of the corresponding broad and unstructured spectra. Again, the effective length scales indicate which influences dominate the numerical results. In this stage the nonlinearity N^2 is similar to the precompression fiber, explaining the very rapid spectral broadening. At the end of the fiber the effective length scale for TOD gets as short as L_{TOD} = 4.3 mm. Thus propagation is dominated by linear dispersion without further nonlinear compression.

#103469 - $15.00 USD Received 30 Oct 2008; revised 11 Dec 2008; accepted 11 Dec 2008; published 15 Jan 2009

We now compare these predictions with an experimental implementation. The measured dispersion profiles of the PF and HNF are given in Fig. 5(b). Fig. 5(a) shows the calculated spectrum for these fibers for a realistic pump pulse envelope and phase (black dots). As depicted in Fig. 1 the fiber output is sent through an SF10 prism sequence which compensates for the GVD of optical components after the fiber end facet while keeping higher-order phase errors moderate. The spectrum we record (blue line) is in good agreement with the simulation. It features a width of λ_{FWHM} = 560 nm at a central wavelength of 1.17 μm which translates to a frequency bandwidth of ν_{FWHM} =110 THz. The compressed pulses feature an energy of 0.7 nJ at a repetition rate of 49 MHz. In order to characterize the pulse duration we design a Mach-Zehnder type autocorrelator with metallic beamsplitters and reflective focussing, detecting the two-photon signal from a InGaP photodiode. The autocorrelation is given as a blue line in Fig. 5(c). A numerical calculation based on the measured spectrum and a fitted 4th order polynomial phase is indicated by the dots. We extract a temporal width of $t_{\mathrm{FWHM}} = (7.8 \pm 1.0)$ fs from this fit corresponding to only 2 optical cycles. To our knowledge these are the shortest pulses generated in an all-fiber setup up to now. This result may be considered as an upper limit set by the bandwidth of the nonlinear photodetector as indicated by a time-bandwidth product of 0.86. The spectral width even supports pulses with transform-limited durations as short as 5.4 fs.

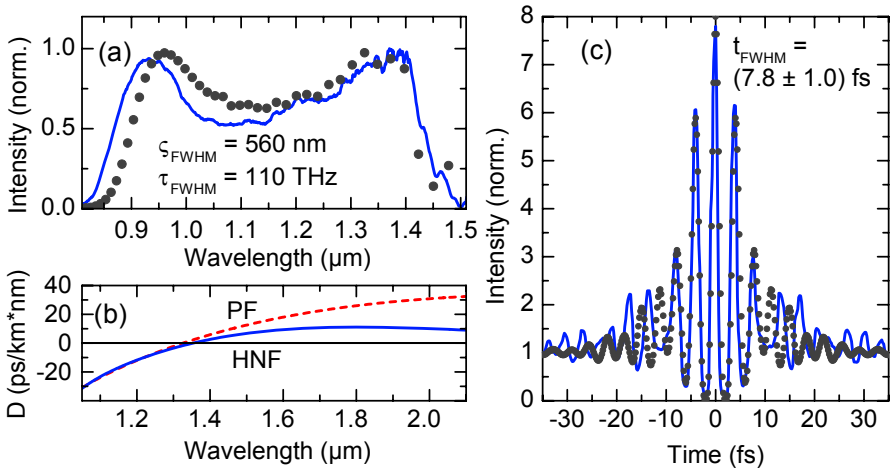

Fig. 5. (a) Parameter free simulation of the output spectrum for experimentally determined pump spectrum and dispersion properties of the optimized fiber compressor (black dots) and measured output spectrum (blue line) vs. wavelength; (b) dispersion D of the pre-compression fiber PF (red, dashed) and the highly nonlinear fiber HNF (blue line) vs. wavelength; (c) autocorrelation of the output pulses after recompression in an SF10 prism compressor (blue line) and simulated trace (black dots) derived from the spectrum and a polynomial phase fit.

Finally we investigate the noise properties of the entire fiber system. Fig. 6 depicts the rms amplitude noise spectrum of our ultrashort pulses (red line) as detected with an InGaAs photodiode. The low-frequency window ranging from 1 Hz to 100 kHz is covered by an FFT spectrum analyzer (Stanford Research Systems SR780) whereas the components up to the Nyquist frequency of 24.5 MHz are recorded using a radio frequency spectrum analyzer (Advantest R3463). For the entire frequency interval from 3 Hz to 24.5 MHz the excess rms amplitude noise is below 10^{-5} $\mathrm{Hz}^{-1/2}$ despite the strong nonlinearity of our setup. A remarkable feature

#103469 - $15.00 USD Received 30 Oct 2008; revised 11 Dec 2008; accepted 11 Dec 2008; published 15 Jan 2009

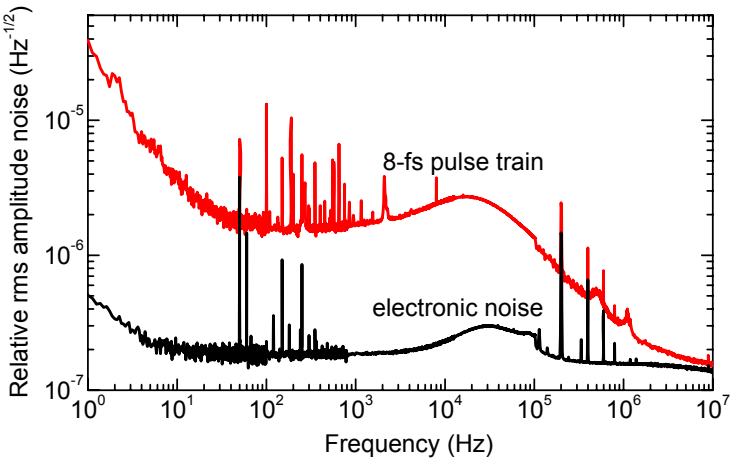

Fig. 6. Relative rms amplitude noise spectrum of an ultrabroadband continuum from a HNF (red line) after compression to a pulse duration of 8 fs and corresponding electronic detection noise floor (black line).

of the supercontinuum is its low rms amplitude noise in the typical audio frequency lock-in detection range between 10 Hz and 10 kHz. It amounts to less than 3×10^{-6} Hz$^{-1/2}$ except for some harmonics of the line frequency of 50 Hz and sharp acoustic resonances.

5. Conclusion

In conclusion we have elaborated a realistic modeling of the pulse compression in two-stage bulk fiber setups. The model is initialized with experimental parameters and therefore offers outstanding predictive power without adjustable fit parameters. First applications include the generation of tunable near IR pulses in the spectral range from 856 nm up to 1450 nm and the development of an all fiber source for two-cycle pulses of a duration of 7.8 fs. The entire laser system is extremely compact (less than 0.5 m^2 footprint), offers turn-key operation, and excellent amplitude and timing noise characteristics. It is easily extendable to multiple output ports synchronized to the attosecond level [14]. Since each branch may be equipped with a different HNF, it is possible to have various wavelengths and pulse widths from one laser setup at the same time. We believe this system to be an ideal source for a wide range of applications regardless whether they require few cycle seed pulses, multiple phase synchronized outputs at adjustable wavelengths, or tunability throughout the visible and near infrared spectral regimes.

This work has been supported by the Federal Ministry for Education and Research (BMBF) and TOPTICA Photonics AG.

#103469 - $15.00 USD Received 30 Oct 2008; revised 11 Dec 2008; accepted 11 Dec 2008; published 15 Jan 2009